13. SITE 972[1]

Shipboard Scientific Party[2]

HOLE 972A

Date occupied: 25 April 1995

Date departed: 26 April 1995

Time on hole: 23 hr

Position: 35°46.797′N, 18°43.515′E

Bottom felt (drill-pipe measurement from rig floor, m): 3942.0

Distance between rig floor and sea level (m): 11.4

Water depth (drill-pipe measurement from sea level, m): 3930.6

Total depth (from rig floor, m): 4037.4

Penetration (m): 95.4

Number of cores (including cores having no recovery): 10

Total length of cored section (m): 95.4

Total core recovered (m): 93.5

Core recovery (%): 98.0

Oldest sediment cored:
Depth (mbsf): 95.40
Nature: nannofossil clay
Earliest age: late Pliocene

Principal results: Mechanical failure in drilling contributed to this site not fulfilling its objective to investigate accretion-related tectonic processes on the outer toe of the Hellenic accretionary wedge. Minor tilting and local reverse faulting were the only structural features of interest noted. The various turbidite types present may shed light on depositional processes in and around the Ionian Abyssal Plain. However, the microfossils are reworked and poorly preserved and the sediments can be dated only approximately as late Pleistocene to late Pliocene in age.

BACKGROUND AND OBJECTIVES

Site 972 is located on the lower part of the deformation front of the western Mediterranean Ridge at a water depth of 3600 m (Fig. 1). The site is one of two intended to characterize tectonic processes operative at the toe of the accretionary wedge. Penetration was limited to 200 m sub-bottom in view of safety concerns related to the possible existence of Messinian evaporite at depth. Specific objectives of drilling at Site 972 were

1. To investigate the structure of the Pliocene-Pleistocene section in relation to the large-scale processes of subduction and accretion operating in the distal part of the Mediterranean accretionary wedge;
2. To use the evidence of small-scale structures in the cores (i.e., faults and debris flows) to shed light on the vertical tectonic history in relation to accretionary processes and to determine if stresses related to subduction and accretion are transmitted into the overlying plate;
3. To make comparisons with the tectonic-sedimentary history of Site 973, which is located slightly higher on the toe of the accretionary wedge, in particular whether diachronism is observable in tectonic processes;
4. To draw comparisons with the toe area of other accretionary wedge settings drilled during Leg 160, specifically the adjacent Calabrian accretionary wedge drilled at Site 964 on the Pisano Plateau and the lower Cyprus slope drilled at Site 968; and
5. To recover an intact Pliocene-Pleistocene section of sapropels that we hoped could be compared with the adjacent Site 964.

GEOLOGICAL SETTING

Site 972 lies on the Outer Deformation Front of the westernmost part of the Mediterranean Ridge accretionary complex (Fig. 2). The southwestern margin of the accretionary complex is bordered by the Ionian (Messina) and Sirte Abyssal Plains. Direct information on the Messina Abyssal Plain was provided by DSDP Site 374 (Shipboard Scientific Party, 1978; Müller et al., 1978). At this locality, the approximately 300-m-thick section of Pleistocene sediments, mainly turbidites, is underlain by approximately 80 of Pliocene deep-sea sediments and a further approximately 80 m of Messinian sediments comprising dolomitic mud and mudstones, gypsum, and anhydrite. In addition, turbidites up to 12 m thick have been cored (Hieke, 1984). The interpretation of single-channel seismic data suggests that thick evaporitic layers in the Messinian are localized in discrete areas separated by structural highs (Avedik and Hieke, 1981). Based on seismic evidence, the Messinian is inferred to be underlain by a very thick sedimentary succession that is ultimately floored by oceanic, or possibly transitional, crust of Mesozoic age (Finetti, 1982).

The nature of the lower deformation front including Site 972 is known mainly from recent SeaBeam and Sea-MARC side-scan sonar surveys (Kastens et al., 1992). Adjacent to the Sirte Abyssal Plain is a ridge and trough topography, with features 1–8 km long and 1–2 km wide, elongated parallel to the deformation front. The features are interpreted as resulting from the effects of accretionary tectonics (i.e., folding and reverse faulting). Kastens et al. (1992) suggested that the dip of the décollement is very low (1.5°–2.5°) and that this could be attributable to the effects of incoming evaporites acting as a lubricant.

By contrast, Hirschleber et al. (1994) pointed out that subduction could induce strong faulting and deformation of the toe of the wedge. It was hoped to test this hypothesis by comparative drilling of Sites 973 and 972. However, it was recognized that the décollement is located at much greater depths than could be penetrated by our drilling.

OPERATIONS

Transit to Site 972

The 304-nmi transit to Site 972 (proposed Site MR-2) required 25.0 hr at 12.2 kt. A 22-nmi seismic survey was run over Sites 972 and 973 in 3.25 hr at 6.8 kt. A Datasonics 354M beacon (S/N 1243, 14.0 kHz) was deployed at Site 972 at 1702 hr on 25 April.

[1]Emeis, K.-C., Robertson, A.H.F., Richter, C., et al., 1996. *Proc. ODP, Init. Repts.*, 160: College Station, TX (Ocean Drilling Program).

[2]Shipboard Scientific Party is given in the list preceding the Table of Contents.

Hole 972A

Hole 972A was spudded at 0150 hr on 26 April. The estimated seafloor was at 3930.6 m by drill-pipe measurement (DPM). APC Cores 160-972A-1H through 7H were taken from 0 to 66.5 mbsf, with 66.5 m cored and 66.70 m recovered (100.3% recovery; Table 1). The last three cores were partial strokes with imploded liner bottoms, and Core 160-972A-7H had a 70,000-lb pullout. The bottom 2–3 m of Cores 160-972A-6H and 7H were suck-in. ADARA heat-flow measurements were taken on Cores 160-072A-5H and 7H.

XCB Cores 160-972A-8X through 10X were taken from 66.5 to 95.4 mbsf, with 28.8 m cored and 26.84 m recovered (93.2% recovery). The XCB core barrel would not land properly for Core 160-972A-11X. When it was pulled, we found that the Spring-Hex Quick Release Adapter had backed off the spring shaft, leaving the XCB core barrel in the open hole below the female Hex Drive. The spring shaft threads were undamaged and it was reused. The hole was terminated, and the BHA was pulled, clearing the seafloor at 1602 hr on 26 April.

Hole 972B

A new XCB latch assembly and core barrel were made up. Hole 972B was spudded at 1655 hr on 26 April in 3930.6 m water depth to continue coring. An XCB wash barrel was dropped, and a hole was drilled from 0 to 60.1 mbsf to obtain a missing APC core suck-in section. The wash barrel was pulled with about 2 m of wash core recovered. An APC core barrel was run, but it would not pressure up to shoot. Assuming some wash core had been dropped in the barrel, an XCB core barrel was pumped down as a deplugger. The XCB landed with low pump pressure and was worked without success. There was no visible damage to the core barrels; therefore, the BHA was pulled, clearing the seafloor at 2258 hr on 26 April. The beacon was recovered.

SITE GEOPHYSICS

A single seismic line was run across Site 972 from east to west (Fig. 3). The presence of small-scale relief in deep water makes the acquisition of good seismic data difficult; thus, the seismic data display many diffractions and little penetration or resolution (Fig. 4). Using both the echo-sounder records and the seismic data, in conjunction with a hydrosweep multibeam bathymetric map that was made during earlier site surveys, it was possible to identify some of the hills and valleys on the seafloor.

The site is located on a topographic high in a region of the lower distal part of the Hellenic accretionary prism where the relief is in the range of only tens of meters. The hill is at a water depth of 3820 m (uncorrected) with small basins containing ponded sediments on both sides at depths of 3845 and 3840 m to the west and the east, respectively. The small basins are part of a series of basins that are progressively shallower from the Ionian Basin to the west, at depths of about 4000 to 4100 m. The hills, or ridges, as many appear to be from the multibeam bathymetric map, are on the order of only 100 m or so wide; the intervening basins, or valleys, vary from less than 100 m to about 200 m in the region surveyed.

Some deeper reflectors were observed, but they are difficult to interpret because they are broken up by diffractions and because the survey was not long enough to build a coherent picture of larger scale continuity and context. Judging from the location, it was expected that the relief is caused mainly by folding of the surficial sediments in the toe of the accretionary prism and partly by reverse faulting that is probably responsible for the steplike elevation of the abyssal plain turbidites onto and into the accretionary prism. At this level in the accretionary complex, and at this proximity to the abyssal plain, it is most likely that the relief is sufficiently low to allow the accumulation of relatively low-density turbidites.

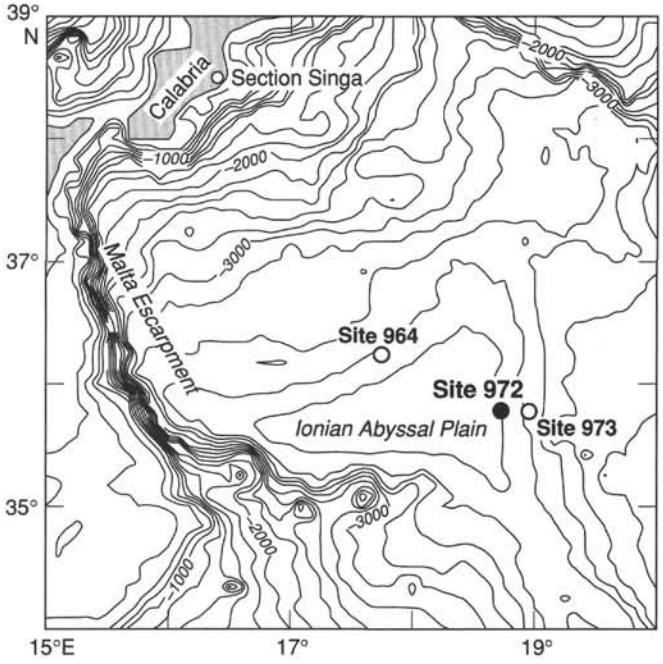

Figure 1. Outline map showing the location of Site 972 on the lower toe of the Mediterranean Ridge accretionary wedge. Note the location of Site 973 slightly higher on the slope and that of Site 964 farther northwest.

LITHOSTRATIGRAPHY

The lithostratigraphic section recovered from the single hole at Site 972 consists of 95.4 m of sediment of latest Pliocene to Holocene age. The composition is dominated by nannofossil clay, clayey nannofossil ooze, and nannofossil ooze. On average, the clay component decreases downsection. The sequence consists of numerous light-colored intervals (generally decimeter to some meter thick) of nannofossil clay, nannofossil ooze, and clayey nannofossil ooze; some are massive, most grade normally, and some are slightly to moderately bioturbated. Faint color banding and mottling are common throughout many of these intervals. The graded beds have been interpreted as fine-grained turbidites. Volcanic glass is disseminated throughout the section.

The dominant light-colored intervals alternate with beds (24 in total) of dark-colored nannofossil clay and clay. All these sapropel beds contain disseminated organic matter and pyrite with variable amounts of volcanic glass, quartz, inorganic calcite, and plant fragments. The dark-colored beds are enriched in organic carbon.

Criteria employed in lithostratigraphic description and classification at Site 972 included (1) visual observation of color; (2) visual observation of sedimentary structures, including bioturbation; (3) smear-slide examination; and (4) carbonate determinations.

Because the dominant lithology of the sequence exhibits little downcore lithologic variation, the sediments were classified as a single lithostratigraphic unit. Within this unit, sapropel and ash are present as minor lithologies. The sedimentological composition of the sapropels within the section is presented within the unit description. A lithostratigraphic summary of Site 972 is shown in Figure 5.

Description of Lithostratigraphic Unit

Lithostratigraphic Unit I

Description: Nannofossil clay, clayey nannofossil ooze, and nannofossil ooze
Intervals: Cores 160-972A-1H through 10X
Depth: 0–95.4 mbsf
Age: latest Pliocene to Holocene

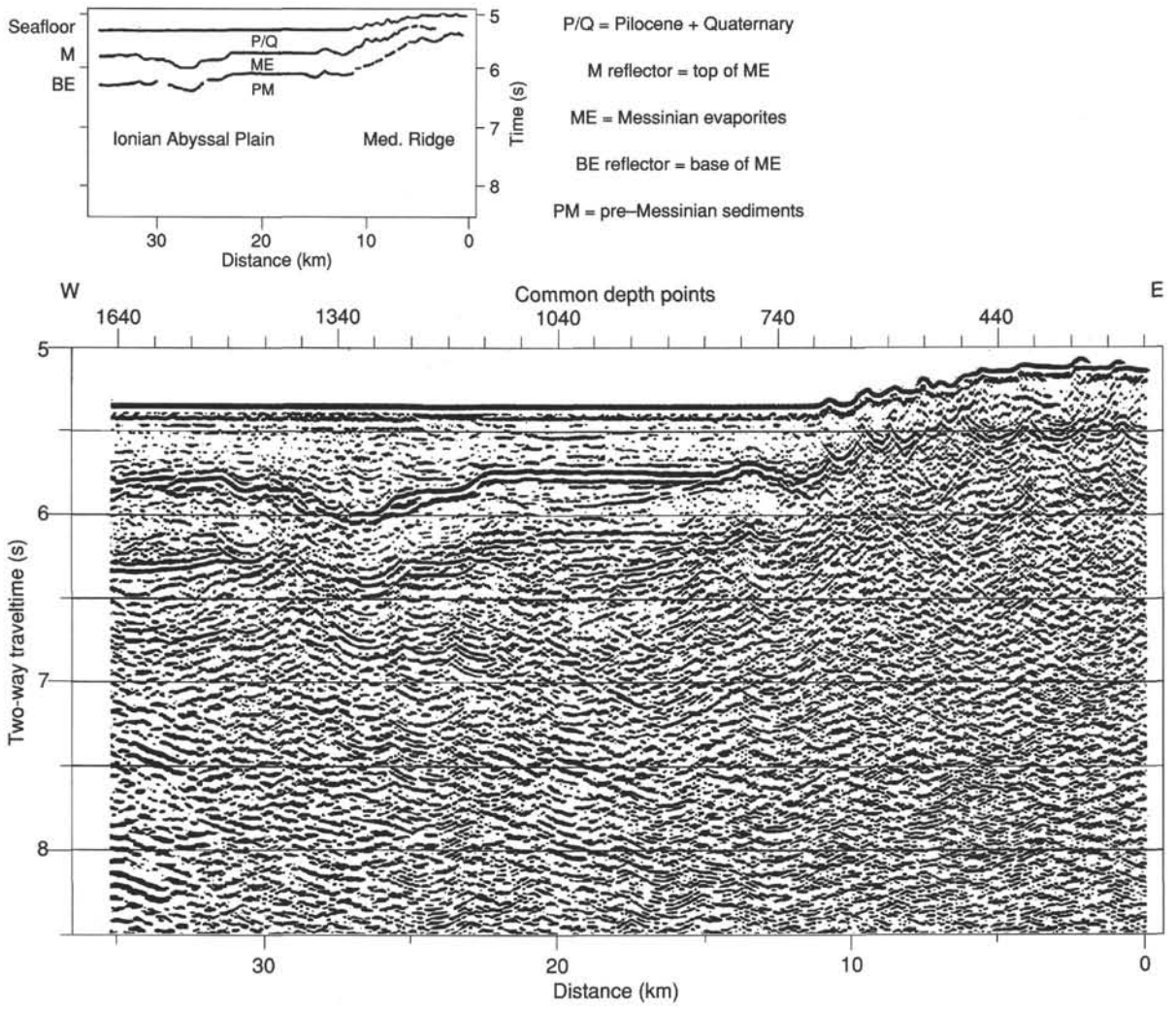

Figure 2. Single-channel seismic profile across the deformation front between the Ionian (Messina) Abyssal Plain and the Mediterranean Ridge shows an east-west profile across the Victor Hensen structure and Site 972. The deformation front is more highly deformed in this area than farther north, possibly owing to the effects of subduction of a locally rough downgoing slab. Inset: line interpretation (from Hirschleber et al., 1994).

Table 1. Coring summary for Site 972.

Core	Date (April 1995)	Time (UTC)	Depth (mbsf)	Length cored (m)	Length recovered (m)	Recovery (%)
160-972A-						
1H	26	0020	0.0–9.5	9.5	9.57	101.0
2H	26	0110	9.5–19.0	9.5	9.75	102.0
3H	26	0205	19.0–28.5	9.5	9.93	104.0
4H	26	0300	28.5–38.0	9.5	9.04	95.1
5H	26	0425	38.0–47.5	9.5	9.15	96.3
6H	26	0530	47.5–57.0	9.5	9.60	101.0
7H	26	0655	57.0–66.5	9.5	9.66	101.0
8X	26	0830	66.5–76.1	9.6	9.82	102.0
9X	26	0940	76.1–85.7	9.6	8.64	90.0
10X	26	1115	85.7–95.4	9.7	8.38	86.4
Coring totals:				95.4	93.5	98.1
160-972B-						
No recovery						

The lithology of Unit I is dominated by alternations of light grayish brown (10YR 5/2), light gray (10Y 6/1), gray (10Y 4/1), and greenish gray (5GY 5/1) nannofossil clay, clayey nannofossil ooze, and nannofossil ooze. Smear-slide analyses reveal that the sediment is composed of between 20% and 80% nannofossils and between 5% and 60% clay. The clay component, on average, decreases downhole. Results of quantitative determination of carbonate indicate fluctuation throughout the unit, ranging from a minimum of about 15% to a maximum of 86%. Organic carbon values in the light-colored interval are between 0.2% and 0.5% (see "Organic Geochemistry" section, this chapter). Minor components include quartz, volcanic glass, inorganic calcite, and authigenic minerals including pyrite.

Turbidites

Many of the light-colored intervals grade normally on a centimeter to decimeter scale, with sporadic larger beds up to 1 m or more in thickness. The basal contacts of many of the turbidite intervals are highlighted by medium- to fine-grained dark greenish gray (5GY 5/1) silts consisting of quartz, mica, inorganic calcite, and foraminifers (Fig. 6). The fine-grained layers are on average 1 to 2 cm thick and range between <0.5 and 6 cm. Sporadic layers of fine sand, up to 50 cm thick, occur scattered through the section.

At least three distinct of turbidite types were recovered at Site 972. A preliminary classification scheme based on color and composition includes those composed of (1) white (10YR 8/1) nannofossil ooze (Fig. 7); (2) green-yellow (5Y 6/4) clayey nannofossil ooze (Fig. 8); and (3) silt or fine sand, fining upward to dark gray-green (5Y 4/1) nannofossil clay.

Many of the latter are relatively thick (~1 m, e.g., Section 160-972A-7H-2) and have erosional bases (Fig. 9).

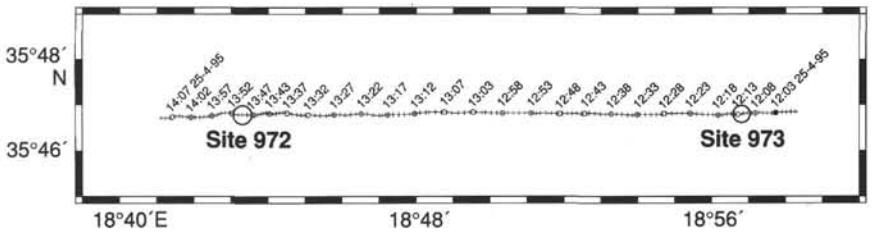

Figure 3. Survey line across both Sites 972 and 973. Seismic profiling was conducted along the full length of the line, but the middle section was run at more than 8 kt and is therefore noisy.

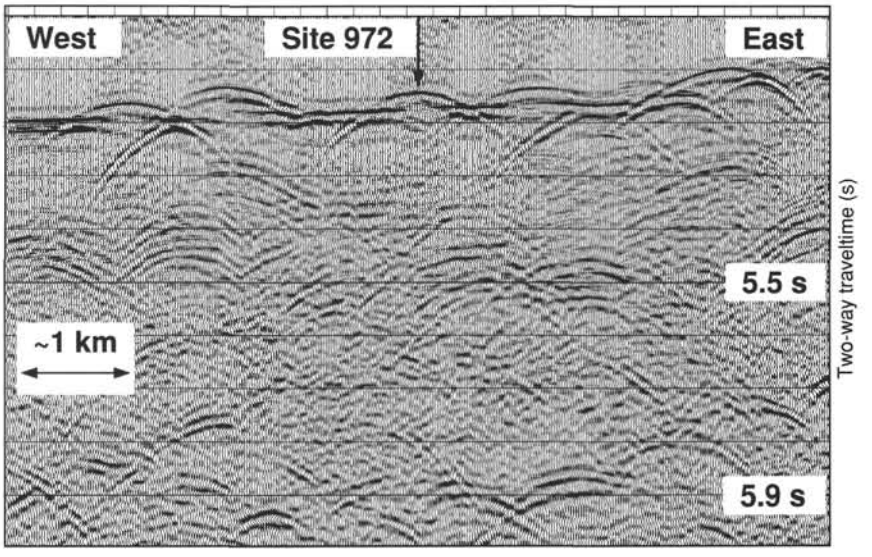

Figure 4. Seismic profile across Site 972. Traces are about 25 m apart.

Sapropels

The dominant background lithology alternates with 24 discrete dark olive gray (5Y 3/2), very dark gray (5Y 3/1), and black (5Y 2.5/1, 2.5/2) beds of nannofossil clay and clay. These sapropels range in thickness from about 1 to 10 cm.

All the sapropels are enriched in pyrite and variable amounts of amorphous organic matter, volcanic glass, quartz, and fragments of higher plant material. Carbonate contents vary considerably (3%–40%) and organic carbon values are between 2% and 15% (see "Organic Geochemistry" section, this chapter).

Traces of burrows cut across boundaries and some beds have intercalated turbidites. Distinctive color zonation (gray and gray-blue) exists close to both the upper and basal contacts of most sapropels. This pattern can be identified in most intervals, even where the organic matter has been oxidized.

Ash

There are several ash layers in the upper part of the core (Fig. 7); several large burrows are also filled with ash (Section 160-972A-1H-3, 0–70 cm). Volcanic glass is also a common minor component of the dominant lithologies, where it probably represents ash layers redistributed and intermixed by bioturbation.

Background and Depositional History

The sequence recovered at Site 972 provides a marine section containing uppermost Pliocene to upper Pleistocene (Holocene) sediments and indicates that the depositional processes and oceanographic conditions in the region have fluctuated since the late Pliocene.

Light-colored, organic-carbon-poor sediments, in particular, the intervals of nannofossil clay, clayey nannofossil ooze, and nannofossil ooze, indicate sedimentation within an oxygenated environment. The depositional style of these materials was predominantly by high-density gravity flow as turbidite pulses with little or no hemipelagic input. The varying composition and character of the turbidites may be indicative of different provenances.

The presence of sapropels suggests a significant change in the flux of organic matter into this area and/or enhanced preservation of organic matter.

BIOSTRATIGRAPHY AND SEDIMENTATION RATES

Calcareous Nannofossils

Calcareous nannofossils were studied primarily from core-catcher samples. To provide a higher resolution biostratigraphy, additional samples were collected from within each core where a zonal boundary was believed to exist. Overall, the cores recovered at this site contain abundant turbidites, which results in an abundance of reworked species. For this reason, the use of zones defined by last appearance datums must be considered tenuous. The samples ranged from late Pleistocene to late Pliocene in age (Fig. 10).

Samples 160-972A-1H, 29 cm, through 2H, 5 cm, are in Zone MNN21a and contain *Emiliania huxleyi* in quantities lower than

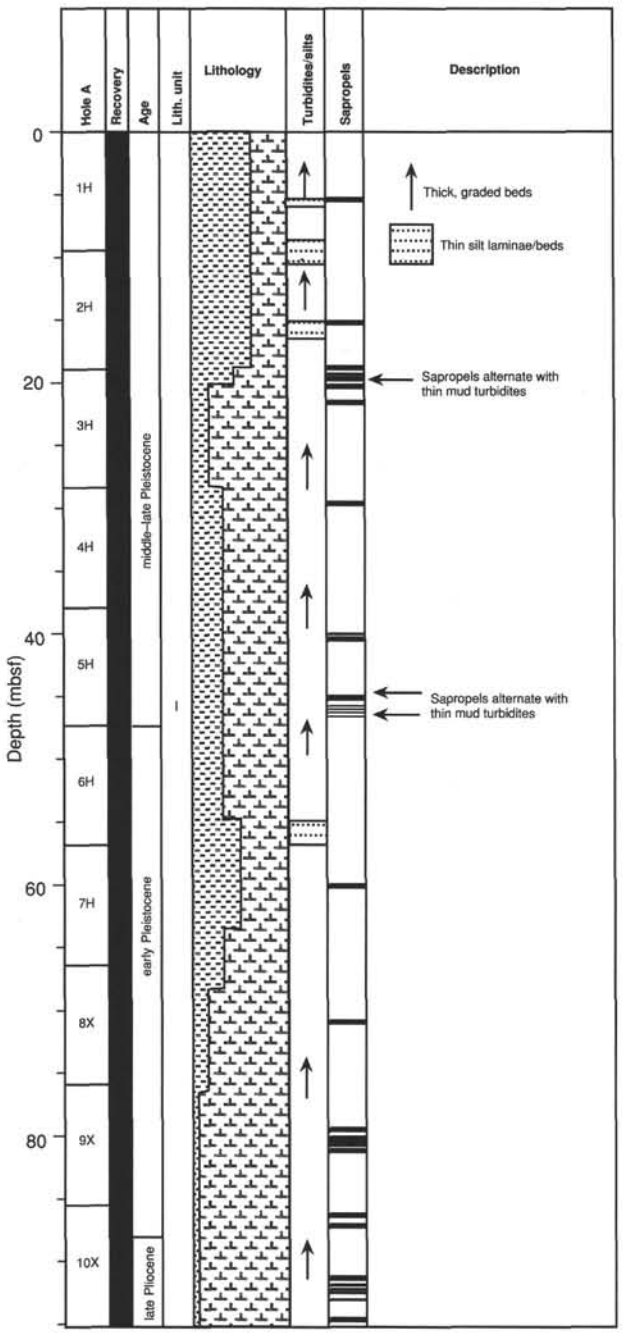

Figure 5. Core recovery, age information, and lithostratigraphic summary for Site 972.

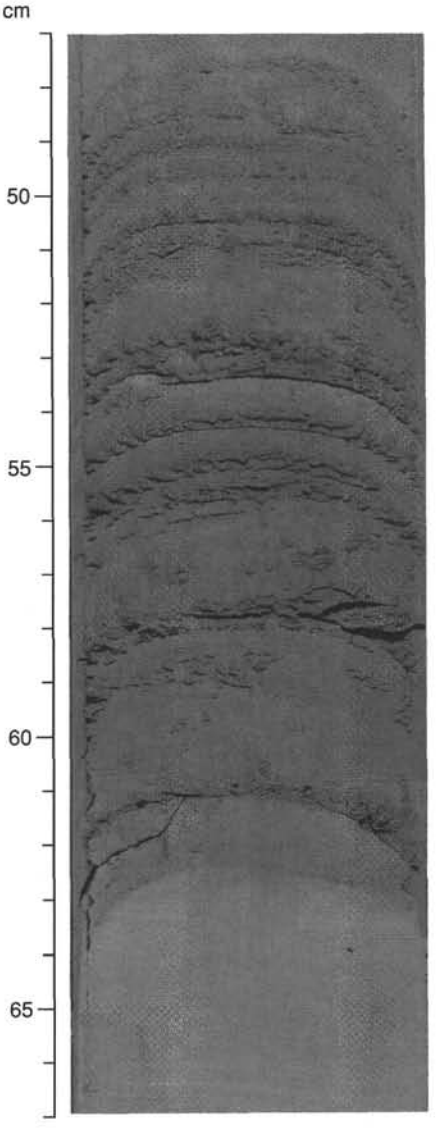

Figure 6. Example of thin (0.5–1.0 cm) silt layers alternating with nannofossil ooze and nannofossil clay (Section 160-972A-1H-6, 47–67 cm).

those of the acme zone, which was not identified upsection. The accompanying assemblage includes small *Gephyrocapsa* (<3.5 µm), *Gephyrocapsa oceanica* s.l., *Helicosphaera kamptneri, Coccolithus pelagicus, Rhabdosphaera clavigera,* and *Pontosphaera japonica.* Reworking fluctuates from rare to common and consists of late Pleistocene, Pliocene, middle Miocene, and Late Cretaceous age taxa.

Samples 160-972A-2H-6, 37 cm, through 4H-1, 104 cm, were placed into Zone MNN20, which is a gap zone defined by the absence of both *E. huxleyi* and *Pseudoemiliania lacunosa.* The accompanying in situ and reworked assemblages are similar to those found uphole.

Samples 160-972A-4H-2, 20 cm, through 6H-6, 142 cm, contain nannofossils from Zone MNN19f. The upper boundary of the zone is defined by the last occurrence of *P. lacunosa,* whereas the lower boundary is defined by the first occurrence of *Gephyrocapsa* sp. 3. The placement of the upper boundary of this zone is difficult because *P. lacunosa* was found in rare abundances in samples uphole. The interpretation of where the top of the zone exists is subjective and based solely upon an increase in abundance of *P. lacunosa* from rare to few. The uphole occurrences are interpreted to be reworked, whereas the samples herein are considered in situ. The in situ and reworked assemblages that accompany *P. lacunosa* are similar to those found uphole. *Gephyrocapsa* sp. 3 is present in Samples 160-972A-5H-5, 73 cm, through 6H-6, 142 cm.

Samples 160-972A-6H-CC, through 9X-6, 10 cm, contain varying quantities of large *Gephyrocapsa* (>5.5 µm), which mark Zone MNN19d. This interval also contains abundant turbidites (see "Lithostratigraphy" section, this chapter) with corresponding reworked nannofossils. The presence of large *Gephyrocapsa* in the samples indicates that the zones immediately above and below Zone MNN19d are not present in Hole 972A. The missing zones (MNN19c and MNN19e) may represent local unconformities resulting from scouring by the turbidites.

Samples 160-972A-9X-CC through 10X-3, 62 cm, contain nannofossils from Zone MNN19b. This zone is identified by the presence of both *G. oceanica* s.l. and *Calcidiscus macintyrei.* The

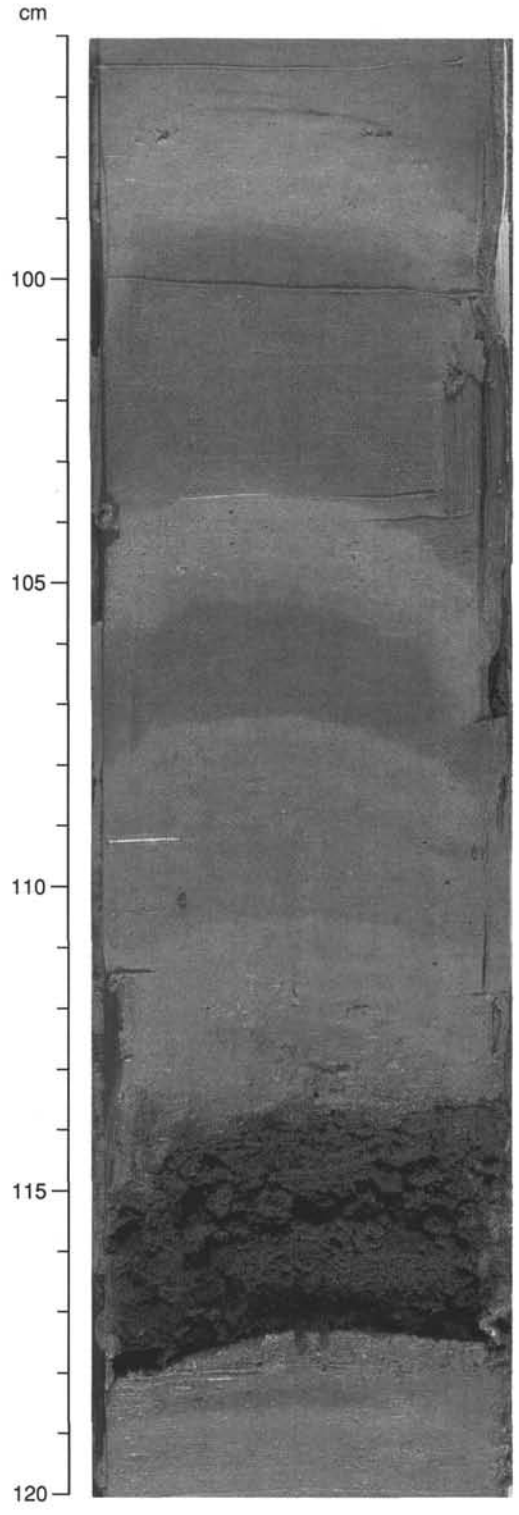

Figure 7. Example of centimeter-scale nannofossil ooze turbidites highlighted by color changes in the sediment (Section 160-972A-1H-4, 96–120 cm). A 3-cm-thick ash layer occurs between 114 and 117 cm.

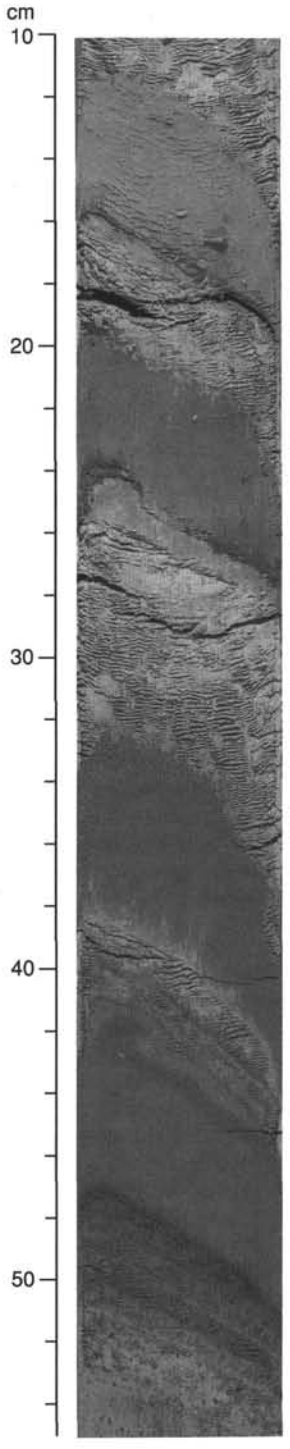

Figure 8. Stacked turbidites (decimeter scale) (Section 160-972A-6H-5, 10–55 cm). Each unit has a silt base and grades into nannofossil clay.

accompanying in situ and reworked assemblages are similar to those found uphole.

Samples 160-972A-10X-4, 40 cm, through 10X-CC contain nannofossils from Zone MNN19a. This zone is identified by the absence of both *G. oceanica* s.l. and *Discoaster brouweri.* The accompanying assemblage is diverse and includes *H. kamptneri,* small *Gephyrcapsa, Syracosphaera pulchra,* and small reticulofenestrids.

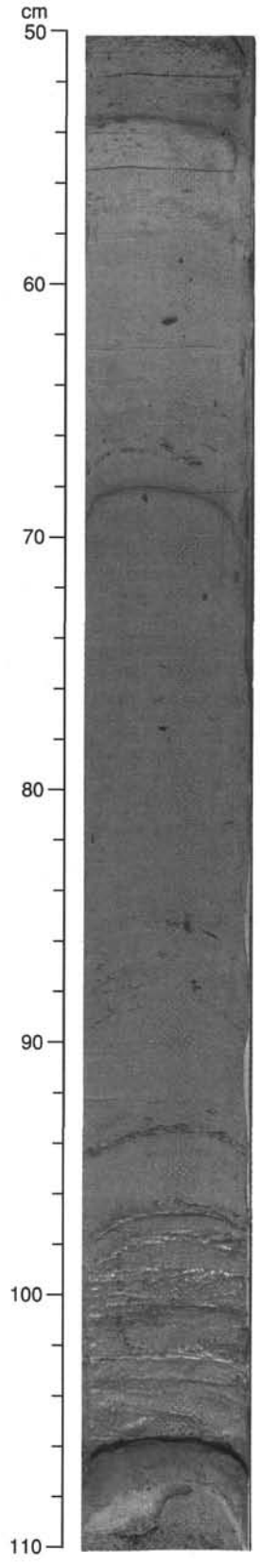

Figure 9. A 45-cm-thick turbidite grading from an erosive-based fine sand (106–97 cm) to nannofossil clay (Section 160-972A-4H-2, 50–110 cm). Internal color bands and flecks are due to diagenesis (pyrite? formation) and redox processes in pore fluids.

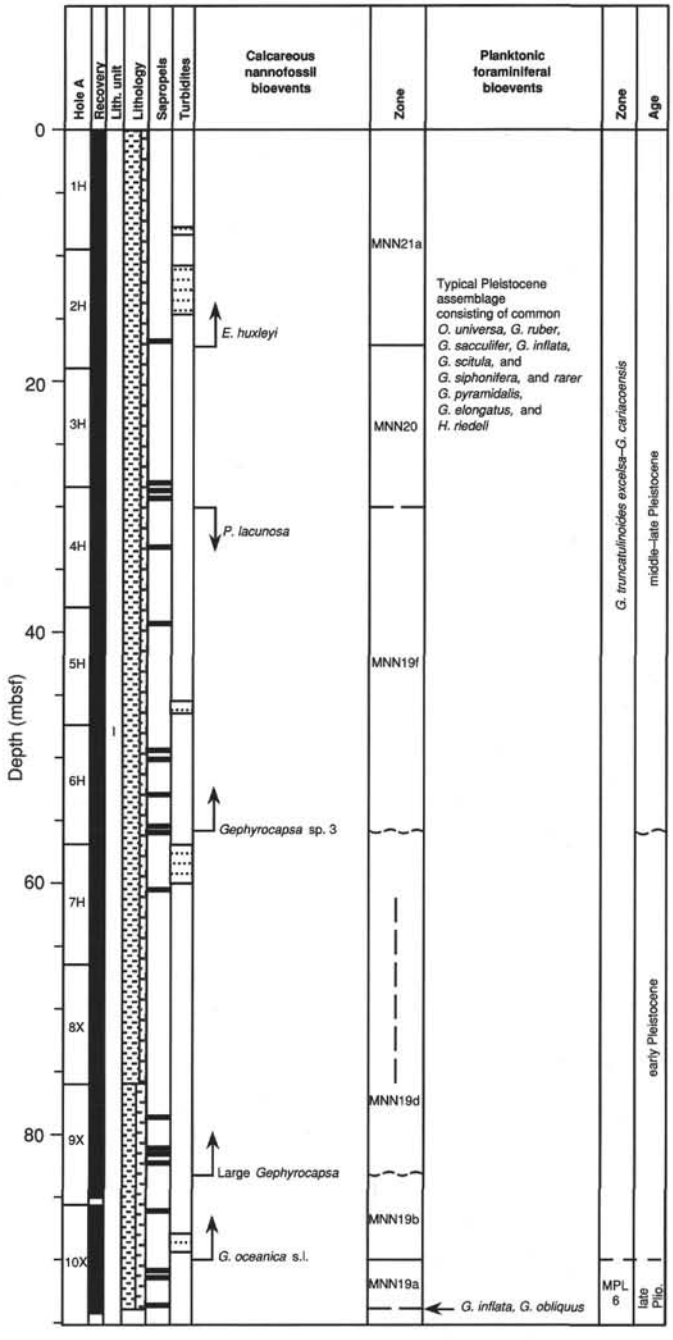

Figure 10. Composite of biostratigraphic events recognized in sediments recovered from Hole 972A including the lithostratigraphic record.

Planktonic Foraminifers

Samples from core catchers and core sections were analyzed for planktonic foraminifers in Hole 972A. Planktonic foraminifers are generally common to abundant and consist of well-diversified and moderately to well-preserved Pleistocene to late Pliocene age faunas (Fig. 10).

The zonal boundary between the *Truncorotalia truncatulinoides excelsa* and *Globigerina cariacoensis* Zones was not recognized owing to the scarcity of *T. truncatulinoides excelsa.* The *T. truncatulinoides excelsa–G. cariacoensis* interval was identified from Samples 160-972A-1H-CC through 10X-5, 100–102 cm. Planktonic foramin-

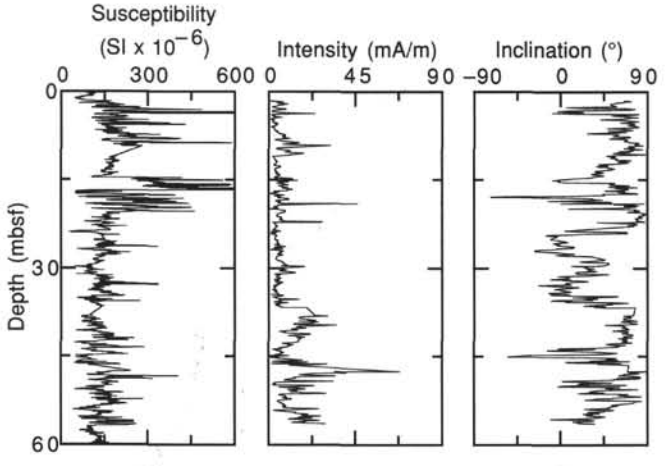

Figure 11. Magnetic susceptibility, paleomagnetic intensity, and inclination for Hole 972A. Inclination and intensity were measured after AF demagnetization at 25 mT.

iferal assemblages are relatively uniform throughout the Pleistocene sequence. Representative taxa include *Orbulina universa, Globorotalia inflata, Globigerinoides ruber, Globorotalia scitula, Globigerina bulloides, Turborotalita quinqueloba, Globigerinita glutinata, Globigerinita juvenilis,* and *Neogloboquadrina pachyderma* (both dextral and sinistral forms). Rare taxa include *Globigerinoides sacculifer, Pulleniatina obliquiloculata, Globigerinoides gomitulus, Globigerinoides pyramidalis, Globigerinoides conglobatus,* and *Hastigerinopsis riedeli.*

Sample 160-972A-10X-CC contains *G. inflata* and the Pliocene species *Globigerinoides obliquus* and was tentatively assigned to Zone MPL6. The accompanying assemblage is similar to those observed in the upper part of the section.

Clear reworking of "older" faunas has affected the planktonic foraminiferal assemblages in a few intervals, in addition to the entire sedimentary sequence (see "Lithostratigraphy" section, this chapter).

Samples 160-972A-1H-CC and 2H-CC contain rare specimens of the early Pliocene age species *Globorotalia margaritae, Globorotalia puncticulata, Globigerinoides extremus,* and *Zeaglobigerina nepenthes.*

Sample 160-972A-9X-CC contains rare specimens of the middle Miocene species *Globigerinoides bisphericus.*

Sedimentation Rates

The sedimentation rates for Hole 972A were not determined. The recovered sediments contain many turbidites that have probably eroded parts of the zones and provided a mechanism to rework microfossils into younger sediments.

Reworking of the nannofossil marker *P. lacunosa* into the uppermost sediments from Hole 972A suggests that this last occurrence datum may not be reliable in Hole 972A. Although the remaining biomarkers recognized are first occurrence datums, the first occurrences of large *Gephyrocapsa* and *Gephyrocapsa* sp. 3 are problematic because of possible unconformities at these events.

PALEOMAGNETISM

Paleomagnetic measurements were restricted to the upper 56 m of Hole 972A (i.e., to the bottom of Core 160-972A-6H). Measurements at Site 972 were routinely made on the archive half of each core section at 10-cm intervals after AF demagnetization at 25 mT. NRM intensities were well above the noise level of the magnetometer throughout the measured interval in Hole 972A (Fig. 11). The overall NRM intensity and magnetic susceptibility records are significantly different. Generally higher intensities occur in the lower part of the measured sequence, whereas higher susceptibilities occur in the upper part of the sequence (Fig. 11). These differences are probably due to stratigraphic variations in the nature of the magnetic (including paramagnetic) mineralogy and could be related to variations in the input of coarse detrital grains. The occurrence of numerous turbidites in Hole 972A (see "Lithostratigraphy" section, this chapter) provides a mechanism for transport and deposition of coarse magnetic grains that generally have high susceptibility and relatively low remanence intensity. Susceptibility peaks were not observed for all of the turbidites seen in the record, which provides evidence that the turbidites may be derived from different source areas. This hypothesis is speculative, however, and must be verified by sedimentological and mineralogical analyses. The whole-core inclination profile determined from Hole 972A is dominated by normal polarity (Fig. 11). The paleontological data indicate that the bottom of the sequence measured is associated with the first occurrence of *Gephyrocapsa* sp. 3 (see "Biostratigraphy and Sedimentation Rates" section, this chapter), which is dated at 0.99 Ma in the Mediterranean area (Sprovieri, 1993). This suggests that the Matuyama/Brunhes boundary and the Jaramillo Subchron should be observed in this record. These polarity zones are not evident in the whole-core record. The large number of turbidites within this sequence complicates the record and may contribute to the ambiguous polarity record. Insufficient time was available to measure the required number of discrete paleomagnetic samples to elucidate the paleomagnetic behavior at Site 972. The possibility of determining a useful magnetic polarity stratigraphy from Site 972 must therefore be evaluated after detailed post-cruise studies.

STRUCTURAL GEOLOGY

The single hole drilled at Site 972 is located on the southern toe of the Mediterranean Ridge, tens of meters above the abyssal plain (see "Site Geophysics" section, this chapter). Bedding measurements in Cores 160-972A-4H through 7H, which were recovered using oriented APC drilling, indicate that the beds dip to either the northeast or the southwest.

Tilted bedding can be seen on the core face in Cores 160-972-1H, 2H, and 5H through 7H. Three-dimensional investigation, however, revealed that bedding in all of the upper seven cores is tilted at shallow to moderate (11°–57°) angles (Table 2). When corrected back to geographic coordinates, the data from Cores 160-972A-4H through 7H dip dominantly toward the southwest with a subsidiary component that dips toward the northeast (Fig. 12A).

Only three faults were observed throughout the entire APC-drilled section (Table 2). These were found in Core 160-972A-7H, where they have small reverse offsets of 0.5–2 cm (Fig. 13). Correction to geographic coordinates reveals that they dip toward the northwest (Fig. 12B).

Cores 160-972A-8X through 10X were recovered by XCB drilling. These cores contain abundant chevronlike structures (e.g., Sections 160-972A-8X-3, 15–35 cm, 8X-4, 15–50 cm, and 8X-5, 25–110 cm) that can be explained by drilling-induced biscuiting. Evidence of rotation prohibited the measurement of structures relative to the core liner.

Little interpretation can be made on such a limited data set. However, the apparent systematic orientation of bedding to the southwest and northeast is consistent with the broad northwest-southeast strike of the Mediterranean Ridge. The changes in orientation within cores (e.g., Core 160-972A-5H), however, are more likely the result of synsedimentary changes in slope associated with turbidite deposition (see "Lithostratigraphy" section, this chapter). The reverse faulting, though limited, may be related to the compressional tectonic setting of the Mediterranean Ridge.

Table 2. Structural data collected at Site 972.

Core, section, interval (cm)	Depth (mbsf)	Feature	Offset width (cm)	Orientation on core face (degrees)		Second apparent orientation (degrees)		Calculated orientation (degrees)		Geographic orientation (degrees)		Comments
				Apparent dip	Direction	Apparent dip	Direction	Dip	Direction	Dip	Direction	
160-972A-												
1H-4, 27	4.77	SB		0	90	25	0	25	0			
1H-4, 47–54	4.97	F		52	90	Not visible						Synsedimentary faulting
1H-4, 56–60	5.06	SB		30	270	21	0	35	304			
1H-4, 87	5.37	SB		0	90	22	0	22	0			
2H-5, 53–55	16.03	SB		28	90	0	180	28	90			
2H-5, 62–63	16.12	SB		6	90	33	0	33	9			Erosive surface
2H-5, 64–67	16.14	SB		40	90	39	0	49	46			
2H-5, 95–96	16.45	SB		33	90	7	0	33	79			
4H-4, 70	33.7	SB		0	90	22	0	22	0	22	69.5	Base of turbidite
5H-1, 7	38.07	SB		0	90	0	0	0	0	0	8.5	
5H-1, 125–127	39.25	SB		10	90	20	0	22	27	22	35.5	
5H-2, 34–37	39.84	SB		18	90	17	0	24	47	24	55.5	
5H-2, 144–146	40.94	SB		11	90	20	0	22	28	22	36.5	
5H-3, 44–46	41.44	SB		13	90	20	0	22	30	22	38.5	
5H-4, 41–43	42.91	SB		15	90	12	0	19	52	19	60.5	
5H-5, 13–15	44.13	SB		13	270	0	0	13	270	13	278.5	
5H-5, 24–26	44.24	SB		20	270	13	0	23	238	23	246.5	
5H-5, 30–32	44.30	SB		23	270	9	180	24	250	24	258.5	
5H-6, 77–82	46.27	SB		32	90	17	180	40	48	40	56.5	
5H-6, 98–103	46.48	SB		34	90	29	180	41	51	41	59.5	
6H-1, 95–97	48.45	SB		27	270	24	0	34	311	34	203.5	
6H-3, 126–129	51.76	SB		29	270	31	0	39	317	39	209.5	
6H-5, 99–104	54.49	SB		26	270	6	0	27	282	27	174.5	
6H-6, 13–18	55.13	SB		34	270	2	0	34	272	34	164.5	Sharp base of turbidite
6H-6, 88–92	55.88	SB		36	270	9	0	37	282	37	174.5	
6H-7, 27–31	56.77	SB		31	270	2	0	31	273	31	165.5	
7H-1, 91–92	57.91	SB		17	270	15	0	22	311	22	189.5	
7H-3, 6–11	60.06	SB		41	270	21	0	44	294	44	172.5	Purple band
7H-3, 37–61	60.37	F	0.5	9	90	0	342	9	72	9	310.5	Reverse fault
7H-3, 43–68	60.43	F	1.2	10	90	0	338	11	68	11	306.5	Reverse fault
7H-4, 46–50	61.96	SB		46	270	49	0	57	318	57	196.5	Color change
7H-4, 104–115	62.54	F	2	47	90	16	0	48	75	48	313.5	Reverse fault

Note: Feature symbols defined in Table 2 ("Explanatory Notes" chapter, this volume).

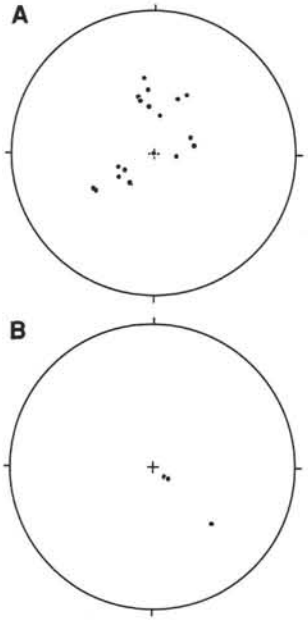

Figure 12. **A.** Equal-area lower hemisphere plot of the distribution of poles to bedding planes from Cores 160-972A-3H through 7H with respect to geographic coordinates. **B.** Equal-area lower hemisphere plot of the distribution of poles to reverse faults from Core 160-972A-7H with respect to the geographic coordinates.

ORGANIC GEOCHEMISTRY

Volatile Hydrocarbons

As part of the shipboard safety and pollution-prevention monitoring program, hydrocarbon gases were analyzed in each core of Hole 972A by the headspace technique. Only minor concentrations of methane in the range of 2 to 93 ppm were recorded. The results are reported in Table 3. Methane concentrations were constantly low down to about 40 mbsf. Below this depth, there was an increase of methane concentration down to Core 160-972A-9X and a decrease again in the deepest core.

Carbon, Nitrogen, and Sulfur

The abundances of total, inorganic, and organic carbon, calcium carbonate, and total nitrogen and sulfur in sediments from Hole 972A are summarized in Table 4. Random sampling was performed for Hole 972A, with additional samples taken from the dark sapropels.

Carbonate contents are quite variable and range from 3% in a black sapropel to 68% in a background nannofossil ooze (Fig. 14). Carbonate contents are low in those sapropels richest in organic matter (>5% C_{org}) in Sections 160-972A-2H-5, 2H-CC, and 5H-6, but otherwise are in the range of the adjacent background sediment.

Organic carbon values in Hole 972A are highly variable both in sapropels and in background sediments (Table 4, Fig. 14). The maximum value of 14.4% was measured in Sample 160-972A-2H-5, 134–135 cm.

C_{org}/N ratios in sapropels vary from 11.8 to 18.3 (disregarding the oxidized sapropel in Section 160-972A-1H-2, which has a slightly lower value; Table 4). As already observed at previous sites (see "Organic Geochemistry" section in the chapters for Sites 964 and 966–969, this volume), the surprisingly high values of the C_{org}/N ratio in many of the sapropels suggest a predominance of terrestrial organic

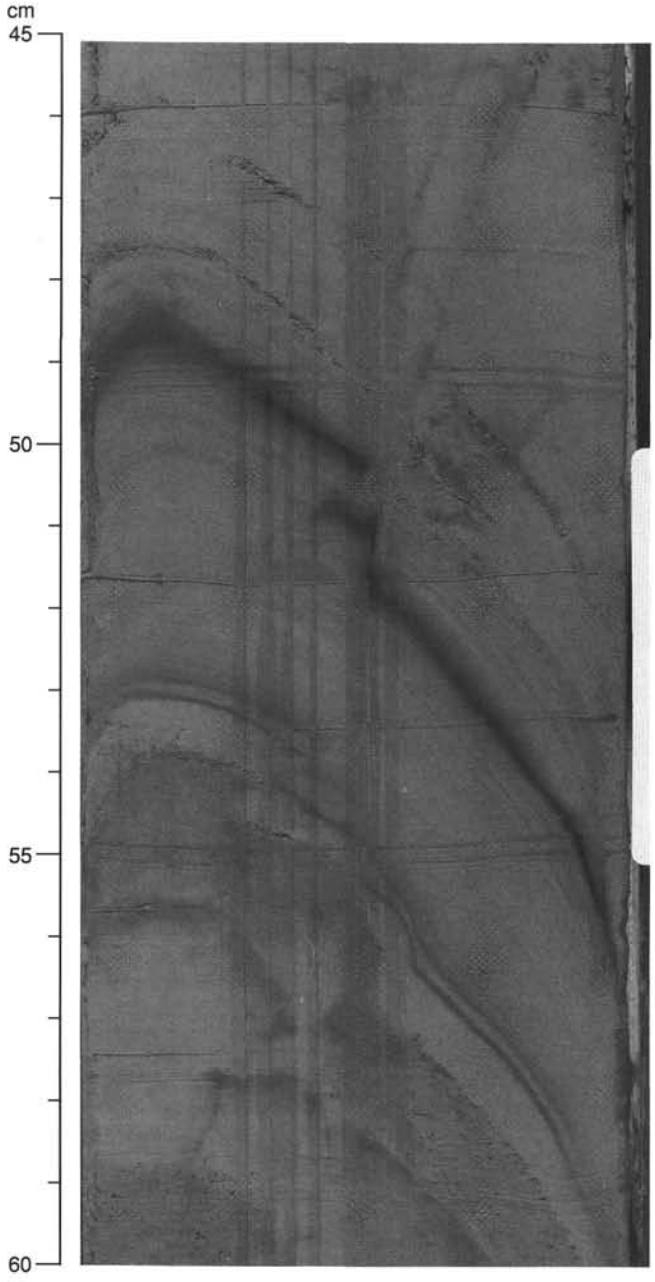

Figure 13. Example of reverse faulting from Section 160-972A-7H-3, 45–60 cm.

matter. The high C_{org}/N ratios in the sapropels are again tentatively interpreted as representing an effective removal of nitrogen compounds from the marine organic matter during diagenesis. However, the possibility that the primary marine organic matter was already poor in nitrogen-bearing constituents cannot be excluded.

Sulfur values are reported in Table 4. Sulfur concentrations vary from 1% to almost 5% in the sapropels, but are not closely related to organic carbon content. An exception is the oxidized sapropel in Section 160-972A-1H-2, which apparently is free of sulfur.

PHYSICAL PROPERTIES

A nearly complete suite of physical and index properties (see "Explanatory Notes" chapter, this volume) was measured in all cores from Hole 972A. Thermal conductivity measurements were cancelled to allow early splitting and description of the cores. In this section, we describe the downhole distribution of physical properties in Hole 972A.

Table 3. Hydrocarbon gas data for Hole 972A, headspace method.

Core, section, interval (cm)	Depth (mbsf)	C_1 (ppm)
160-972A-		
1H-5, 0–5	6.00	3
2H-5, 0–5	15.50	3
3H-5, 0–5	25.00	4
4H-5, 0–5	34.50	5
5H-5, 0–5	44.00	15
6H-5, 0–5	53.50	33
7H-5, 0–5	63.00	42
8X-5, 0–5	72.50	48
9X-5, 0–5	82.10	93
10X-4, 0–5	90.10	37

Index Properties

Bulk and dry density were measured in every section of the unconsolidated sediment down to 60 mbsf. Density generally increases with depth (Table 5, Fig. 15). The abrupt increase followed by a constant decrease between 8 and 16 mbsf is probably an artifact resulting from core expansion. This pattern also occurs in the GRAPE measurements (see below). A large variation within 2 m, which appears at about 35 mbsf, is attributed to probable suction.

Discrete-sample *P*-wave and Shear Strength Measurements

Horizontal and vertical *P*-wave velocities measured with the digital sonic velocimeter show a generally increasing trend with depth in Hole 972A from 1.5 to 1.8 km/s (Table 6, Fig. 16). Vane shear strength shows a similar pattern with depth, ranging between 20 and 100 kPa (Table 7, Fig. 16).

GRAPE Density

The overall trend of the GRAPE data (Fig. 17) is toward slightly increasing density to a depth of 60 mbsf. The hard clays that were sampled by XCB show lower density values down to 95 mbsf. A comparison of the index properties density measurements (Fig. 17) with GRAPE density suggests that the GRAPE measurements in this hole underestimate density by approximately 1.5 g/cm^3, despite application of the Boyce correction (see "Explanatory Notes" chapter, this volume, and as discussed in the "Physical Properties" section, "Site 967" chapter, this volume).

Compressional Wave Velocities

High-resolution compressional wave velocities were measured using the PWL of the MST (Fig. 18). The velocity increases with depth from 1.5 to 1.8 km/s at a constant rate over the measured interval. At 10 mbsf, both methods show a local maximum of velocity.

Magnetic Susceptibility

Figure 19 shows the results of magnetic susceptibility measurements from Hole 972A. The values increase from the seafloor to 10 mbsf and then slowly and steadily decrease. On a finer scale, considerable variation can be observed where the zone of abundant sapropels at 80–95 mbsf is distinguished by intensive susceptibility fluctuations.

Table 4. Concentration of total, inorganic and organic carbon, calcium carbonate, total nitrogen, and sulfur in sediments from Hole 972A.

Core, section, interval (cm)	Depth (mbsf)	Total carbon (%)	Inorganic carbon (%)	Organic carbon (%)	$CaCO_3$ (%)	Nitrogen (%)	Sulfur (%)	C_{org}/N	C_{org}/S
160-972A-									
1H-2, 48–49	1.98	5.72	4.10	1.62	34.15	0.16	0.00	10.1	
1H-2, 60–61	2.10		1.77		14.74				
1H-2, 115–116	2.65		2.34		19.49				
1H-4, 70–71	5.20		1.80		14.99				
1H-6, 69–70	8.19		2.65		22.07				
2H-2, 90–91	11.90		6.37		53.06				
2H-4, 90–91	14.90		3.56		29.65				
2H-5, 110–111	16.60	2.65	2.42	0.23	20.16	0.05	0.00		
2H-5, 134–135	16.84	14.81	0.41	14.40	3.42	0.88	4.60	16.4	3.1
2H-CC, 9–10	19.15	7.30	1.97	5.33	16.41	0.33	3.48	16.2	1.5
3H-1, 14–15	19.14	7.49	4.44	3.05	36.99	0.22	3.45	13.9	0.9
3H-1, 87–88	19.87	7.26	4.47	2.79	37.24	0.21	2.78	13.3	1.0
3H-3, 44–45	22.44		4.70		39.15				
3H-4, 26–27	23.76	6.19	4.51	1.68	37.57	0.13	1.18	12.9	1.4
3H-6, 44–45	26.94		7.21		60.06				
4H-1, 69–70	29.19	3.16	2.65	0.51	22.07	0.05	0.15	10.2	3.4
4H-1, 132–131	29.82	6.33	4.21	2.12	35.07	0.18	3.57	11.8	0.6
5H-1, 61–62	38.61		8.17		68.06				
5H-2, 114–115	40.64	7.34	5.00	2.34	41.65	0.18	2.74	13.0	0.9
5H-4, 90–91	43.40		4.85		40.40				
5H-6, 45–46	45.95	8.47	1.16	7.31	9.66	0.40	2.93	18.3	2.5
6H-1, 100–101	48.50		4.43		36.90				
6H-4, 99–100	52.99		3.65		30.40				
7H-2, 80–81	59.30		6.93		57.73				
7H-3, 16–17	60.16	7.76	5.06	2.70	42.15	0.19	3.69	14.2	0.7
7H-4, 79–80	62.29		6.52		54.31				
7H-4, 134–135	62.84	11.37	3.88	7.49	32.30	0.43	4.41	17.4	1.7

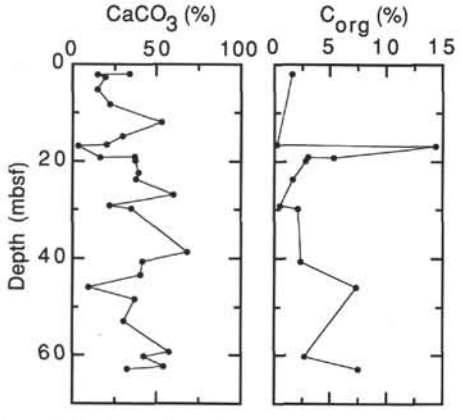

Figure 14. Downhole distribution of calcium carbonate and organic carbon concentrations for samples from Hole 972A.

Natural Gamma-ray Radiation

NGR values measured using the MST from Hole 972A show several first-order trends (Fig. 20). Similar to the susceptibility, the NGR values increase from the seafloor to 10 mbsf and then slowly and steadily decrease. Between 62 and 66 mbsf is a local maximum.

Correlation with Lithostratigraphy

The change in sediment consolidation at 60 mbsf is well recorded by the GRAPE measurements. Indications of this change, and the change to the sapropel-rich interval below 80 mbsf, are discernible in the magnetic susceptibility and NGR records.

HEAT-FLOW MEASUREMENTS

In situ temperatures were measured with the ADARA system on Cores 160-972A-5H and 7H (Table 8, Fig. 21). All time-temperature series were of high quality and no disturbance was observed during the temperature measurements. The average temperature gradient is constant at about 28 K/km. Thermal conductivity values from the core measurements (see "Physical Properties" section, this chapter) are not available. Using estimated values of 1.2 W/(m · K) at 47.5 mbsf and 1.3 W/(m · K) at 66.5 mbsf, the heat flow was calculated as 30–32 mW/m^2 for the upper 70 m at Site 972.

SUMMARY AND CONCLUSIONS

Drilling at Site 972 was aimed at shedding light on subduction-accretion processes in an area where the Ionian Abyssal Plain is being subducted under the Mediterranean Ridge accretionary complex. The objectives were not achieved, largely because of a mechanical failure in drilling that did not allow penetration below 100 mbsf. Sediments were dated as late Pleistocene to latest Pliocene, but most microfossils are reworked and preservation is poor. The sediments comprise three main types of fine-grained turbidites, locally with thin silty graded bases. Typical Pleistocene and Pliocene sapropels are interbedded. The sediments are locally tilted and show minor evidence of reverse faulting.

The results from Site 972 suggest that turbidites accumulated on, or near, the Ionian Abyssal Plain and were locally tilted and deformed within the distal toe of the Mediterranean Ridge accretionary complex.

REFERENCES

Avedik, F., and Hieke, W., 1981. Reflection seismic profiles from the Central Ionian Sea (Mediterranean) and their geodynamic interpretation. *"Meteor" Forschungsergeb. Reihe C,* 34:49–64.

Finetti, I., 1982. Structure, stratigraphy and evolution of central Mediterranean. *Boll. Geofis. Teor. Appl.,* 24:247–315.

Hieke, W., 1984. A thick Holocene homogenate from the Ionian Abyssal Plain (Eastern Mediterranean). *Mar. Geol.,* 55:63–73.

Hirschleber, H.B., Hartmann, J.M., and Hieke, W., 1994. The Mediterranean Ridge accretionary complex and its forelands—seismic reflection studies in the Ionian Sea. *Cruise Report of the Meteor,* 120:491–509.

Kastens, K.A., Breen, N.A., and Cita, M.B., 1992. Progressive deformation on an evaporite-bearing accretionary complex: SeaMARC 1, SeaBeam, and piston-core observations from the Mediterranean Ridge. *Mar. Geophys. Res.,* 14:249–298.

Table 5. Index properties measured in cores from Hole 972A.

Core, section, interval (cm)	Depth (mbsf)	Water content (wt%)	Porosity (vol%)	Bulk density (g/cm³)		Grain density (g/cm³)		Dry density (g/cm³)	
				Method B	Method C	Method B	Method C	Method B	Method C
160-972A-									
1H-1, 64–66	0.64	38.87	63.15	1.73	1.66	3.05	2.76	1.05	1.02
1H-2, 93–95	2.43	43.63	66.66	1.62	1.57	2.93	2.65	0.91	0.88
1H-3, 24–26	3.24	43.99	67.50	1.61	1.57	2.90	2.71	0.90	0.88
1H-4, 130–132	5.80	40.57	64.65	1.69	1.63	3.03	2.74	1.00	0.97
1H-5, 110–112	7.10	40.04	64.12	1.69	1.64	3.00	2.74	1.01	0.98
1H-6, 111–113	8.61	27.72	52.61	1.51	1.94	1.84	2.97	1.09	1.41
2H-1, 79–81	10.29	41.14	65.07	1.67	1.62	3.00	2.73	0.98	0.95
2H-2, 77–79	11.77	28.30	50.87	1.90	1.84	2.87	2.69	1.36	1.32
2H-3, 77–79	13.27	30.35	53.68	1.87	1.81	2.91	2.72	1.30	1.26
2H-4, 122–124	15.22	35.67	59.32	1.75	1.70	2.88	2.69	1.13	1.10
2H-5, 43–45	15.93	38.32	61.42	1.72	1.64	2.99	2.63	1.06	1.01

Only part of this table is reproduced here. The entire table appears on the CD-ROM (back pocket).

Müller, J., Hieke, W., and Fabricius, F., 1978. Turbidites at Site 374: their composition, provenance and paleobathymetric significance. *In* Hsü, K.J., Montadert, L., et al., *Init. Repts. DSDP*, 42 (Pt. 1): Washington (U.S. Govt. Printing Office), 397–400.

Shipboard Scientific Party, 1978. Site 374; Messina Abyssal Plain. *In* Hsü, K.J., Montadert, L., et al., *Init. Repts. DSDP*, 42 (Pt. 1): Washington (U.S. Govt. Printing Office), 175–217.

Sprovieri, R., 1993. Pliocene–early Pleistocene astronomically forced planktonic Foraminifera abundance fluctuations and chronology of Mediterranean calcareous plankton bio-events. *Riv. Ital. Paleontol. Stratigr.*, 99:371–414.

Ms 160IR-113

NOTE: Core-description forms ("barrel sheets") and core photographs can be found in Section 5, beginning on page 535. Forms containing smear-slide data can be found in Section 6, beginning on page 951. Color reflectance, physical properties, chemistry, and thin-section data are presented on the CD-ROM (back pocket).

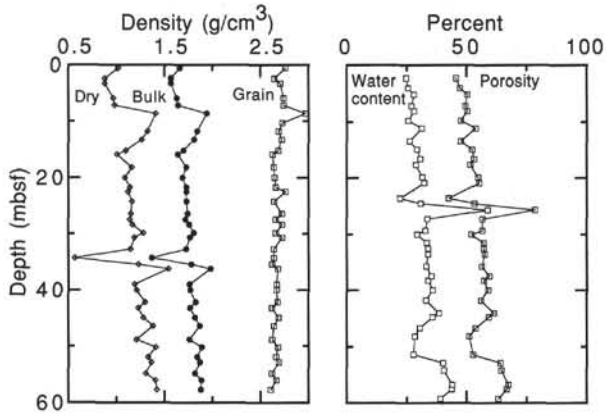

Figure 15. Index properties measured in cores from Hole 972A. Density was calculated using method C (see "Explanatory Notes" chapter, this volume).

Table 6. Compressional wave velocity measured in split cores from Hole 972A.

Core, section, interval (cm)	Depth (mbsf)	Measurement type	Velocity (km/s)
160-972A-			
1H-3, 22.7	3.23	DSV 1	1.51
1H-4, 126.8	5.77	DSV 1	1.53
1H-4, 126.8	5.77	DSV 1	1.53
1H-5, 106.9	7.07	DSV 1	1.52
1H-6, 109.1	8.59	DSV 1	1.57
2H-1, 80.1	10.30	DSV 1	1.53
2H-2, 127.7	12.28	DSV 1	1.62
2H-4, 132.1	15.32	DSV 1	1.55
2H-5, 40.6	15.91	DSV 1	1.57
2H-6, 107.4	18.07	DSV 1	1.57

Note: Direct DSV measurements.

Only a part of this table is reproduced here. The entire table appears on the CD-ROM (back pocket).

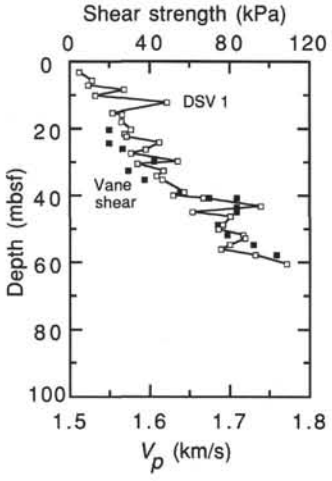

Figure 16. Compressional wave velocity (DSV 1) and shear strength measured in cores from Hole 972A.

Table 7. Vane shear strength measured in split cores from Hole 972A.

Core, section, interval (cm)	Depth (mbsf)	Strength (kPa)
160-972A-		
3H-1, 133.9	20.34	19.80
3H-4, 95.2	24.45	19.80
3H-5, 120.8	26.21	26.50
4H-1, 136.3	29.86	42.30
4H-3, 113.3	32.63	29.60
4H-5, 94.4	35.44	37.40
5H-1, 117.7	39.18	55.30
5H-2, 127.4	40.77	69.80
5H-2, 129.4	40.79	83.70
5H-4, 107.1	43.57	83.70

Only part of this table is reproduced here. The entire table appears on the CD-ROM (back pocket).

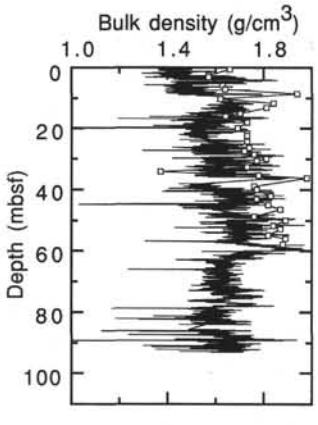

Figure 17. Density measured as part of the index properties measurements (connected open symbols) and GRAPE density (line) measured using the MST.

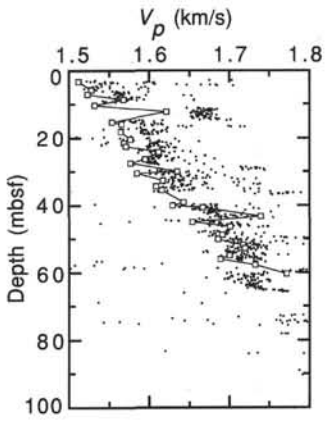

Figure 18. Compressional wave velocities measured in cores from Hole 972A using the PWL component of the MST (solid symbols) and using the DSV (connected open symbols).

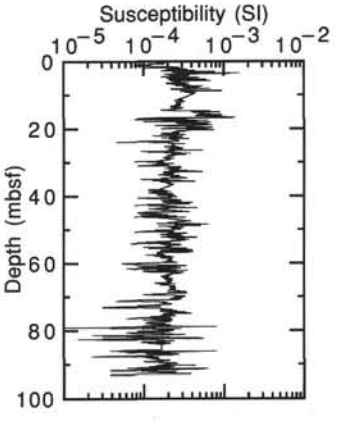

Figure 19. Magnetic susceptibility measured using the MST in cores from Hole 972A.

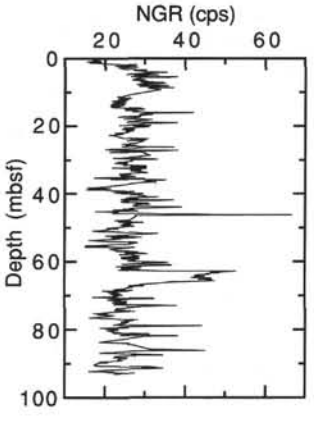

Figure 20. Natural gamma-ray radiation measured in cores from Hole 972A.

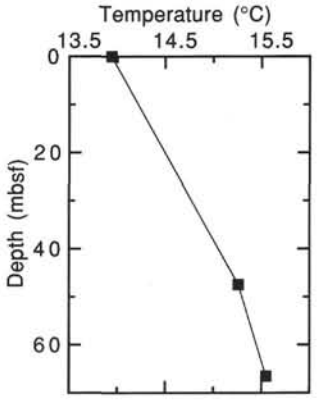

Figure 21. Results of ADARA measurements in Hole 972A.

Table 8. In situ formation temperature measurements made with the ADARA at Hole 972A.

Core	Depth (mbsf)	Temperature (°C)
160-972A-		
Mud line	0.0	13.94
5H	47.5	15.26
7H	66.5	15.55